PHILOSOPHICAL TRANSACTIONS A

rsta.royalsocietypublishing.org

Research

Cite this article: Qian S *et al*. 2016 Elastocaloric effect in CuAlZn and CuAlMn shape memory alloys under compression. *Phil. Trans. R. Soc. A* **374**: 20150309.
http://dx.doi.org/10.1098/rsta.2015.0309

Accepted: 7 April 2016

One contribution of 16 to a discussion meeting issue 'Taking the temperature of phase transitions in cool materials'.

Subject Areas:
materials science, mechanical engineering

Keywords:
elastocaloric effect, CuAlZn, CuAlMn, shape memory alloy, refrigeration

Author for correspondence:
Ichiro Takeuchi
e-mail: takeuchi@umd.edu

†These authors contributed equally to this study.

THE ROYAL SOCIETY PUBLISHING

Elastocaloric effect in CuAlZn and CuAlMn shape memory alloys under compression

Suxin Qian[1,†], Yunlong Geng[2,†], Yi Wang[2], Thomas E. Pillsbury[3], Yoshiharu Hada[5], Yuki Yamaguchi[5], Kenjiro Fujimoto[5], Yunho Hwang[4], Reinhard Radermacher[4], Jun Cui[6], Yoji Yuki[7], Koutaro Toyotake[8] and Ichiro Takeuchi[2]

[1]Department of Refrigeration and Cryogenic Engineering, School of Energy and Power Engineering, Xi'an Jiaotong University, Xi'an, Shaanxi, People's Republic of China
[2]Department of Materials Science and Engineering, [3]Department of Aerospace Engineering, and [4]Center for Environmental Energy Engineering, Department of Mechanical Engineering, University of Maryland, College Park, MD, USA
[5]Department of Pure and Applied Chemistry, Faculty of Science and Technology, Tokyo University of Science, Noda, Chiba, Japan
[6]Department of Materials Science and Engineering, Iowa State University, Ames, IA, USA
[7]Japan Copper Development Association, Tokyo, Japan
[8]Shinko Metal Products Co. Ltd, Fukuoka, Japan

YG, 0000-0002-3590-4769

This paper reports the elastocaloric effect of two Cu-based shape memory alloys: $Cu_{68}Al_{16}Zn_{16}$ (CuAlZn) and $Cu_{73}Al_{15}Mn_{12}$ (CuAlMn), under compression at ambient temperature. The compression tests were conducted at two different rates to approach isothermal and adiabatic conditions. Upon unloading at a strain rate of $0.1\,s^{-1}$ (adiabatic condition) from 4% strain, the highest adiabatic temperature changes (ΔT_{ad}) of 4.0 K for CuAlZn and 3.9 K for CuAlMn were obtained. The maximum stress and hysteresis at each strain were compared. The stress at the maximum recoverable strain of 4.0% for CuAlMn was 120 MPa, which is 70% smaller than that of CuAlZn. A smaller hysteresis for the CuAlMn alloy was also obtained, about 70% less compared with the CuAlZn alloy. The latent heat, determined by differential scanning calorimetry, was

4.3 J g^{-1} for the CuAlZn alloy and 5.0 J g^{-1} for the CuAlMn alloy. Potential coefficients of performance (COP$_{mat}$) for these two alloys were calculated based on their physical properties of measured latent heat and hysteresis, and a COP$_{mat}$ of approximately 13.3 for CuAlMn was obtained.

This article is part of the themed issue 'Taking the temperature of phase transitions in cool materials'.

1. Introduction

Caloric effects refer to the entropy changes when applied external fields, such as stress, electric or magnetic fields, change. In most cases, the entropy changes originate from the first-order phase transition. Recently, owing to the strong demand for efficient and environmentally friendly refrigeration technologies, materials with giant caloric effects, including magnetocaloric [1–3], electrocaloric [4,5], barocaloric [6–8] and elastocaloric [9–12], have been widely investigated.

Elastocaloric cooling, also known as thermoelastic cooling, has been recognized as a promising alternative to the state-of-the-art vapour compression cooling system, owing to the high temperature change [13] within a large temperature span [14] and excellent coefficients of performance (COPs). Elastocaloric cooling is based on the latent heat associated with the austenite–martensite phase transformation in shape memory alloys (SMAs). The exothermic austenite–martensite transformation would cause a temperature increase when the stress is beyond the critical transformation stress. Upon unloading, the reverse martensite–austenite phase transformation will occur, resulting in temperature decrease. A highest temperature change of 17 K was observed in NiTi wires under tension [13]. Experimental measurements of temperature changes in other SMAs, including Ni-Fe-Ga [15] (8.4 K), Co-Ni-Al [15] (3.1 K), Cu-Al-Zn [14] (6 K), Fe-Rh [16] (5.2 K), Cu-Al-Ni [17] (14 K) and Cu-Al-Sn [18] (12 K) under tension and Ni-Fe-Ga-Co [19] (10 K) under compression, have been reported in the literature.

Cu-Al-Zn SMAs, inexpensive and abundant, were reported to have large entropy change [20] (ΔS) and potentially large adiabatic change of temperature (ΔT_{ad}) during phase transformation. A ΔT_{ad} of 14 K under tension test was estimated from its latent heat and specific heat [9], and a significant $\Delta T_{ad} \sim 6$ K was measured by Mañosa *et al.* under tensile tests [14]. In addition, Cu-Al-Zn has been demonstrated to have a superior COP to Ni-Ti as a result of its significantly low hysteresis. Pseudoelastic Cu-Al-Mn SMAs have been used as damping materials, pipe couplings and mechanical fasteners in the past [21,22], owing to their excellent reversible strain of 5% and low critical transformation stress. By adjusting the alloy composition and heat treatment conditions, the transition temperature of Cu-Al-Mn SMAs could be tuned from 93 K to approximately 500 K [23]. At low Al contents, the Cu-Al-Mn SMAs have good ductility and could be cold worked [24]. Therefore, Cu-Al-Zn and Cu-Al-Mn SMAs are promising as elastocaloric materials.

In our previous work [25], an elastocaloric cooling system using Ni-Ti as the refrigerant was designed under compression mode. Because of the relatively high cost of Ni-Ti SMAs, we are exploring Cu-based SMAs as substitutes. Cu-based SMAs are known to display a robust shape memory effect and low critical transformation stress. To apply Cu-based SMAs in the system in the future, it is necessary to investigate their elastocaloric performance under compression.

2. Experimental procedure

A polycrystalline Cu-Al-Zn alloy was prepared by melting high-purity (more than 99.97%) Cu, Al and Zn elements in an induction furnace with an Ar atmosphere. The as-melted ingot was homogenized at 900°C for 1 h, followed by water quenching. It was then boiled in water for 30 min and cooled down in ambient atmosphere. Following this step, the sample was annealed at 500°C

for 1 h, followed by water quenching, to obtain the high-temperature β phase. The composition was determined by wavelength-dispersive X-ray spectroscopy (WDS), which was 68 at.% Cu, 16 at.% Al and 16 at.% Zn.

The Cu-Al-Mn alloys with compositions of $Cu_{72}Al_{17}Mn_{11}$ and $Cu_{82}Al_{14}Mn_4$ were prepared by arc melting. Homogenization at 1000°C for 30 min followed by water quenching was done for each ingot. To obtain the best thermodynamic property, heat treatment at temperatures of 400°C, 500°C, 600°C, 700°C, 800°C and 900°C for different periods of 10 min, 30 min and 60 min followed by water quenching were conducted separately. One sample out of this series ($Cu_{72}Al_{17}Mn_{11}$) displayed a latent heat of 4.8 J g^{-1}. We also obtained a single-crystal sample of Cu-Al-Mn, which displayed very small critical stress, and we decided to measure various properties of this sample. The sample has a dimension of 152 mm in length and 14.5 mm in diameter. The sample was firstly induction-heated to form polycrystalline Cu-Al-Mn alloy; then abnormal grain growth (AGG) was achieved to form a single crystal (β phase) by cyclic heat treatment without macroscopic deformation. AGG of the β phase was realized by a process of slow cooling from 900°C to 500°C and subsequent heating to 800°C followed by water quenching. The composition was 72.8 at.% Cu, 15.1 at.% Al and 12.1 at.% Mn, measured by WDS.

The sample for differential scanning calorimetry (DSC) analysis was sliced to be 0.2 mm in thickness. The slice was cut into pieces and sealed in aluminium pans. The DSC was conducted in a DSC Q100 system (TA Instruments) at a heating and cooling rate of 10 K min^{-1} in an Ar atmosphere. The sample for compression test was machined to 18 mm in length, with a diameter of 8 mm. The test was conducted with an MTS 810 hydraulic universal testing machine. To measure the *in situ* temperature during compression, two T-type thermocouples were welded to positions one-third and two-thirds the length of the body of the sample. Then, the sample was wrapped by foam insulation 5 mm in thickness to reduce heat loss in the radial direction. Nevertheless, the top and bottom surfaces of the sample can still conduct heat to the loading cell of the MTS system. The CuAlMn sample was loaded at a strain rate of 0.0004 s^{-1} to specific strain, then thermalized for 15 s at constant strain, and unloaded at a strain rate of 0.1 s^{-1} to approach adiabatic conditions. For the CuAlZn sample, both loading and unloading at the strain rate of 0.1 s^{-1} was conducted.

3. Results and discussions

The DSC results are shown in table 1. For the CuAlZn sample, the latent heat (L) was estimated to be 4.3 J g^{-1}, and the martensite start temperature (M_s), the martensite finish temperature (M_f), the austenite start temperature (A_s) and the austenite finish temperature (A_f) are −54°C, −75°C, −52°C and −39°C, respectively. Assuming that the austenite–martensite transformation is under fully adiabatic conditions, the temperature lift could be estimated from the entropy change $\Delta T_{ad} = T\Delta s \cdot c_p^{-1}$, where Δs is the entropy change (latent heat) during austenite–martensite transformation and c_p is the specific heat [26], 0.43 J g^{-1} K^{-1}. The estimated highest temperature lift will be $\Delta T_{ad} = 10$ K. The characteristic temperatures for the CuAlMn alloy were $L = 4.8$ J g^{-1}, $M_s \approx -39$°C, $M_f \approx -52$°C, $A_s \approx -26$°C and $A_f \approx -12$°C. Taking the specific heat as 0.43 J g^{-1} K^{-1} [27], the ΔT_{ad} is calculated to be 11.6 K.

The compression tests in this study were conducted at room temperature (21°C), where both the CuAlZn and CuAlMn samples are in the fully austenite state ($T > A_f$). In figure 1, the stress–strain curves for the CuAlZn alloy (strain ranges from 1% to 3.5%) are shown. At low strains (approx. 1.5%), the stress increases linearly with the strain, corresponding to the elastic response of the austenite phase. Upon unloading, the strain was completely recovered with a small hysteresis, which matches well with the compressive behaviour of elastic metals. Starting from 2% strain, superelastic behaviour characteristic of SMAs was observed, indicated by the slope changes along the loading curves when a critical transformation stress was reached. In the stress–strain curve with the highest strain reaching 3.5%, when the critical transformation stress is around 430 MPa, the stress stays almost constant with strain increasing from 2.7% to

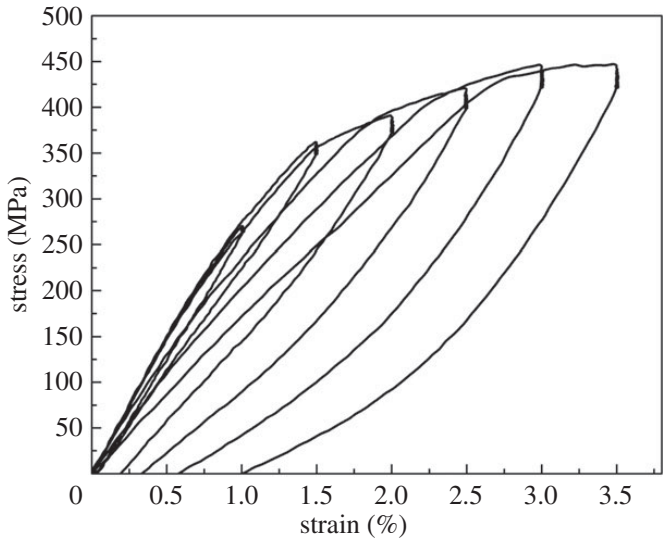

Figure 1. Compressive stress–strain measurements of CuAlZn alloy with strains from 1 to 3.5%.

Table 1. DSC results for CuAlMn and CuAlZn.

materials	composition (at.%)	L (J g^{-1})	M_s (°C)	M_f (°C)	A_s (°C)	A_f (°C)	c_p (J g^{-1} K^{-1})	ΔT_{ad} (°C)
CuAlZn	$Cu_{68}Al_{16}Zn_{16}$	4.3	−54	−75	−52	−39	0.43	10.0
CuAlMn	$Cu_{73}Al_{15}Mn_{12}$	4.8	−39	−52	−26	−12	0.43	11.6

3.5%. This corresponds to the stress-induced transformation from austenite to martensitic phase. Unfortunately, the recovery strain upon unloading gets worse with increasing strains, decreasing from 100% at 1% strain to 71.4% at 3.5% strain. In SMAs, a better recovery could be achieved by training of the stress-induced phase transformation. However, owing to the brittleness of Cu-based SMAs, failure occurs during the training process. Some future work to improve the brittleness of Cu-based SMAs is necessary to enhance the fatigue life and recovery performance during the stress-induced phase transformation.

Compared to the CuAlZn alloy, the CuAlMn alloy starts an austenite–martensite transformation from 2% strain, with a much lower critical transformation stress of 73 MPa (figure 2). With the strain increase to 2.5%, the stress stays almost constant. But starting from 3% strain, the increase of stress with strain indicates the completion of the phase transformation. With further increase of strain to 4%, the characteristic elastic behaviour of the martensitic phase in CuAlMn alloy was observed.

In figure 3, the maximum stress ($stress_{max}$) and hysteresis at each strain for NiTi, CuAlZn and CuAlMn were compared. A detailed description of compressive performance for an NiTi alloy can be found in [25]. As can be seen in figure 3*a*, the highest compressive $stress_{max}$ of 870 MPa at 4% strain was observed in NiTi alloy, while $stress_{max}$ was 450 MPa (nearly half that of NiTi) for CuAlZn, and 130 MPa (one-seventh that of NiTi) for CuAlMn. In figure 3*b*, the largest hysteresis of 0.78 J g^{-1} at 3.5% strain was observed in CuAlZn alloy. Interestingly, the NiTi alloy has a lower hysteresis of 0.51 J g^{-1}, which is due to the excellent recovery upon release of the loading. A minimum hysteresis of 0.20 J g^{-1} was found in the CuAlMn alloy. In the elastocaloric cooling system, both lower $stress_{max}$ and smaller hysteresis are preferred to approach a minimum input energy and highest COP. Therefore, from the mechanical performance aspect, CuAlMn alloy is better than NiTi and CuAlZn alloys. In addition, both the $stress_{max}$ and maximum strain are greatly influenced by A_f. When A_f gets closer to the testing temperature, decrease of $stress_{max}$ would be achieved. Thus, future work on the heat treatment of SMAs is expected to decrease the working stress, and mechanical hysteresis accordingly.

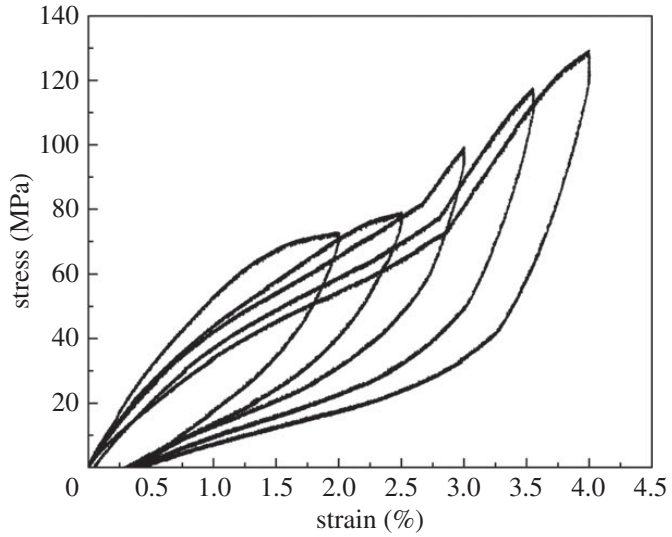

Figure 2. (*a*) Compressive stress–strain measurements of CuAlMn alloy with strains from 2 to 4%.

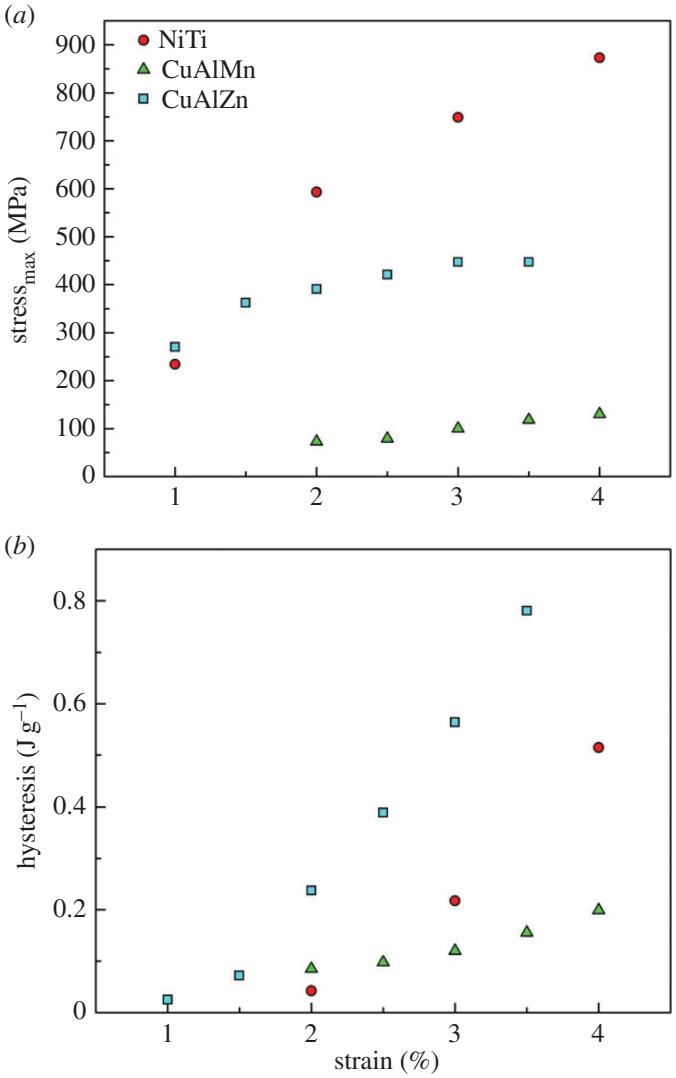

Figure 3. (*a*) Comparison of maximum stress and (*b*) comparison of hysteresis at each strain for NiTi, CuAlMn and CuAlZn. (Online version in colour.)

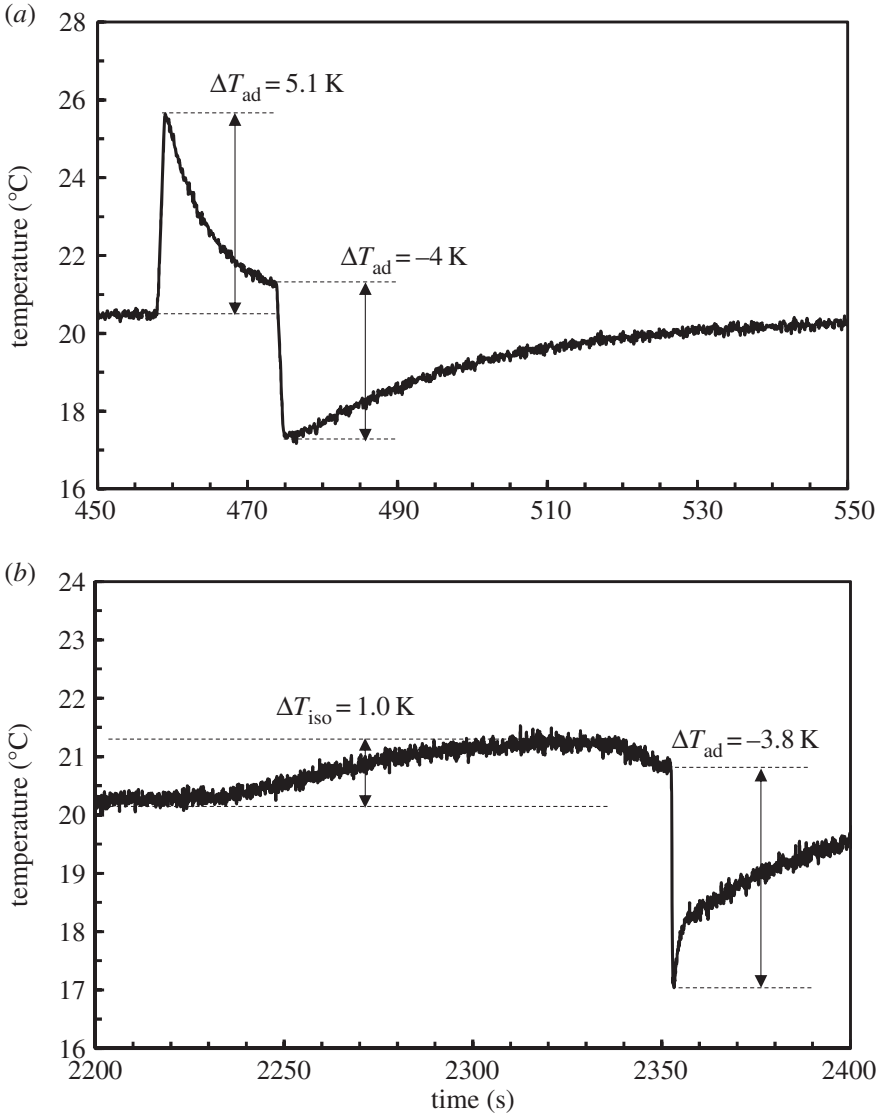

Figure 4. Illustration of temperature variation during the compression test. (*a*) Adiabatic loading and unloading for CuAlZn sample under 3.5% strain. (*b*) Isothermal loading and adiabatic unloading for CuAlMn sample under 3.5% strain.

Figure 4 illustrates the *in situ* temperature variation during the loading and unloading processes. The fast loading rate of $0.1\,s^{-1}$ was to approach the adiabatic condition by minimizing heat loss. The temperature changes for the CuAlZn sample with adiabatic loading and unloading (3.5% strain) is presented in figure 4*a*. The temperature spike was 5.1 K during the loading process, whereas the temperature drop was 4 K upon unloading. The difference between the loading and unloading ΔT_{ad} values is mainly a result of the phase transformation hysteresis, which is fully taken into consideration for the material performance estimation later. The noise in the temperature measurement was due to the high sampling frequency, which was still less than the uncertainty of the T-type thermocouples. Figure 4*b* shows the isothermal loading with adiabatic unloading for the CuAlMn sample under 3.5% strain. Even with the slow loading rate ($0.0004\,s^{-1}$), there was still a 1 K temperature increase during the loading process. Nevertheless, this 1 K variation is small enough to be considered as an isothermal condition. It should be noted that a better control of temperature variation by slower loading rate may result in less hysteresis, and therefore the potential material performance discussed later may be even better.

Figure 5 plots the measured adiabatic temperature drop ΔT_{ad} during the unloading process for both samples under various strains. Upon unloading at 1% strain, a non-trivial ΔT_{ad} around 1 K was detected, indicating the low critical transformation stress. With strains increasing from 1% to

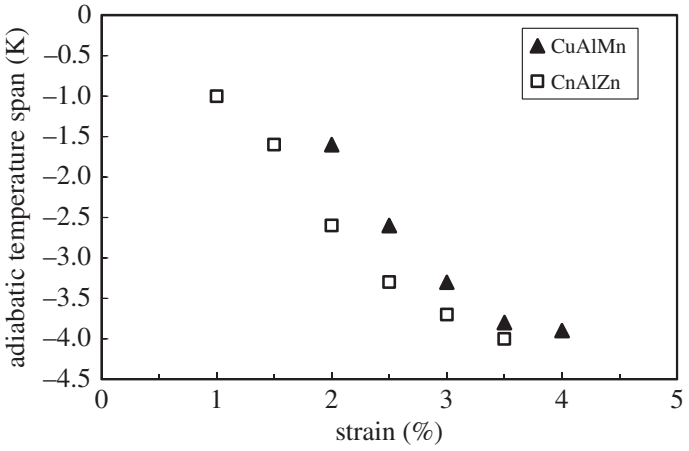

Figure 5. ΔT_{ad} variation at variable strains for CuAlZn and CuAlMn alloys.

3.5%, the temperature drop increases almost linearly to 4 K for CuAlZn, due to the endothermic phase transformation. The maximum ΔT_{ad} were obtained as 4 K for CuAlZn under 3.5% strain and 3.9 K for CuAlMn under 4.0% strain. Compared with the DSC latent heat, which are 4.3 J g^{-1} and 5.0 J g^{-1}, respectively, the theoretical ΔT_{ad} for both materials should be 10.0 K and 11.6 K, respectively. Such a deviation was the result of a few factors. Though heavily insulated in the radial direction, axial heat loss was inevitable due to metal-to-metal conduction from the sample to the steel clamps in the MTS universal testing machine. In addition, the phase transformation was not complete under 3.5% strain or 4.0% strain, but unfortunately no further strains are accessible since the samples could not survive the large deformation under compression mode.

4. Materials evaluation

The CuAlZn sample performance could be evaluated based on a few indices developed from the previous studies [28,29]. The ΔT_{ad} and the latent heat of martensitic transformation are related by $L = c_p \cdot \Delta T_{ad}$. Given an air conditioner as the context, in a real cooling system, the heat rejection temperature (outdoor unit) is higher than the cooling temperature (indoor unit), where the difference is called the system temperature lift ($\Delta T_{lift} = T_{rejection} - T_{cooling}$). As a result, the SMA needs to cool down itself from $T_{rejection}$ to $T_{cooling}$ before providing any useful cooling. Therefore, not 100% of the cooling generated from the martensitic transformation can be harvested, since part of the cooling is used to compensate temperature variation of the SMA itself within each cooling cycle. The first metric, the non-dimensional latent heat ($\gamma = \Delta T_{ad} \cdot \Delta T_{lift}^{-1}$), quantifies the ratio of the useful latent heat of the CuAlZn sample [27]. As shown in figure 5, the ΔT_{ad} of the Cu-Al-Zn sample was measured to be 4 K. As discussed earlier, the direct measure of ΔT_{ad} underestimated the latent heat due to residual heat loss to the metal loading cells, and incomplete phase transformation under 3.5% strain. A second way to estimate ΔT_{ad} is to use the DSC result. By implementing $\Delta T_{ad} = L \cdot c_p^{-1}$ it yields 10.0 K, where L is 4.3 J g^{-1} and c_p is 0.43 J g^{-1} K^{-1}. When using the 10 K ΔT_{lift}, the non-dimensional latent heat γ is found to range from 0.40 to 1.00. Similarly for CuAlMn, the measured ΔT_{ad} is 3.9 K in figure 5. When using the latent heat from DSC results, ΔT_{ad} can be estimated to be 11.6 K, corresponding to γ ranging from 0.39 to 1.16. The value for the state-of-the-art nickel–titanium binary alloy under compression is around 2, and CuZnAl under tensile mode with other compositions can be as high as 1.5 [29].

The second metric is the material-level coefficient of performance (COP_{mat}), defined as the ratio between the useful cooling and the net work required to drive the cycle, assuming the entire unloading energy (area under the unloading curve in figure 1) can be recovered [29]. The COP_{mat} was derived to be a function of the system operating temperatures, entropy change during the martensitic transformation Δs, and a material constant A representing the phase

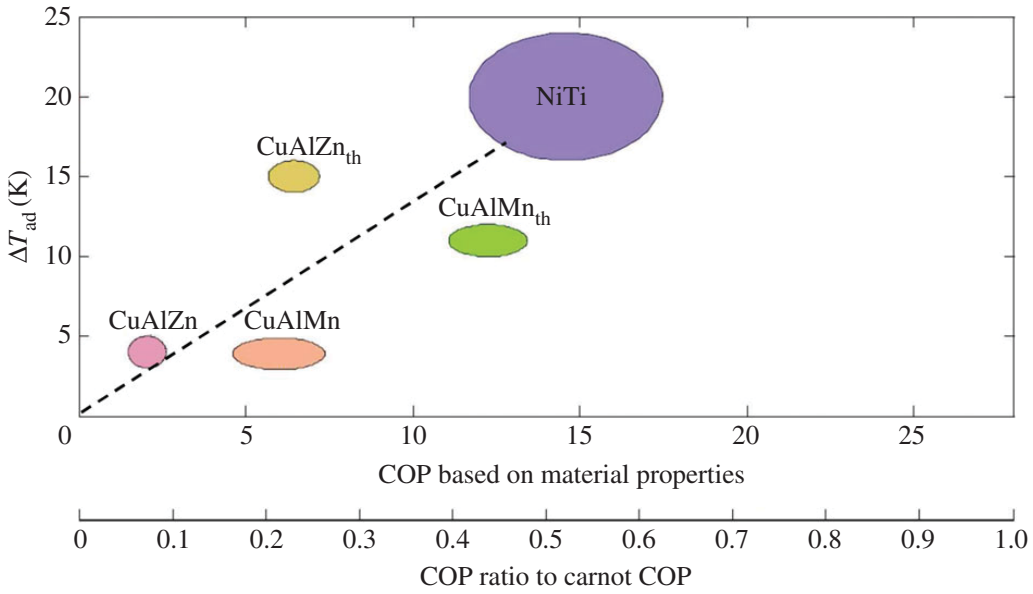

Figure 6. Material COP and adiabatic temperature span for CuAlZn, CuAlMn and NiTi. The subscript 'th' refers to ΔT_{ad} calculated from measured latent heat and heat capacity, and COP calculated from measured latent heat and mechanical hysteresis during loading–unloading process. (Online version in colour.)

change hysteresis, presented as

$$\mathrm{COP}_{mat} = \frac{T_{cooling}\Delta s - A}{\Delta T_{lift} \cdot \Delta s + 2A}. \tag{4.1}$$

In the above equation, if the hysteresis constant A is zero, the COP_{mat} becomes identical to the Carnot cycle COP, which is the theoretical limit of any cooling system based on the second law of thermodynamics. The material hysteresis constant A can be estimated using equation (4.2), if it is adiabatically loaded or unloaded [30], where ρ is the density of the alloy:

$$A = \frac{\left(\int_0^{\varepsilon_{max}} \sigma_{loading} d\varepsilon - \int_0^{\varepsilon_{max}} \sigma_{unloading} d\varepsilon\right)}{2\rho} - \frac{\Delta T_{ad} \cdot \Delta s}{2}. \tag{4.2}$$

The area enclosed by the stress–strain hysteresis loop (at 3.5% strain) in figure 2 is $0.71\,\mathrm{J\,g^{-1}}$. Following equation (4.2), using $\Delta T_{ad} = 4.0\,\mathrm{K}$ and $\Delta s = 0.007\,\mathrm{J\,g^{-1}\,K^{-1}}$ based on measured data, the material hysteresis constant $A = 0.36\,\mathrm{J\,g^{-1}}$, when the system temperature lift $\Delta T_{lift} = 10\,\mathrm{K}$, $T_{cooling} = 288\,\mathrm{K}$, the COP_{mat} for the tested $Cu_{68}Al_{16}Zn_{16}$ sample can be estimated to be 2.0. Similarly, the COP_{mat} based on the measured data for CuAlMn is 6.0, since CuAlMn has a much smaller hysteresis, as shown in figure 3.

As mentioned earlier, owing to unavoidable heat loss from the sample to the loading device and partial phase transformation, the real measured ΔT_{ad} values for both samples are less than those estimated based on the DSC results. Therefore, projections based on theoretical latent heat from DSC are also implemented into equation (4.2) to calculate the theoretical COP_{mat}. The material hysteresis constants remain the same. It yields the COP_{mat} of 6.4 and 12.3 for CuAlZn and CuAlMn samples, respectively. COP_{mat} for NiTi alloy under compression ranges from 15 to 18 [28]. In terms of CuAlZn alloy with other compositions, the COP_{mat} is around 11 under tensile driving mode based on the reported latent heat and stress–strain loop hysteresis.

Figure 6 summarizes the aforementioned results on the COP–ΔT_{ad} chart. Note that another metric on the bottom was based on normalizing the COP_{mat} to the Carnot COP under identical operating conditions, i.e. ΔT_{lift} and $T_{cooling}$. Each ellipse represents the performance of a material when considering the uncertainties in any property measurement, i.e. $\pm 1\,\mathrm{K}$ equivalent ΔT_{ad} uncertainty and $\pm 10\%$ uncertainty in hysteresis calculation. As indicated by equation (4.2), the

two major contributions to COP_{mat} are ΔT_{ad} (or Δs, L) and hysteresis constant A. Being the vertical axis by itself, ΔT_{ad} not only determines the vertical heights for each material, but also contributes to the horizontal positions. The dashed line connecting the origin point and the NiTi ellipse divides the chart domain into two parts: any material located to the right (left) of the line has less (more) hysteresis than NiTi. The measured COP_{mat} for both samples (represented by CuAlMn and CuAlZn in figure 6) are located far away from NiTi in the plot; while assuming the hysteresis to be constant and using the latent heat instead of the measured ΔT_{ad}, the COP_{mat} of CuAlMn (represented by $CuAlMn_{th}$, as ΔT_{ad} is 'theoretical' and not directly measured) is already competitive with that of NiTi. The COP_{mat} of CuAlMn with latent heat based on DSC results correspond to 0.4–0.48 of Carnot COP. Future research to enhance the latent heat of both CuAlZn and CuAlMn is crucial to improve their performance. Methods to strengthen both materials are also essential to access a larger strain in the future so that a fully stress-induced phase transformation can be reached.

5. Conclusion

In this study, the elastocaloric effect of two bulk samples, $Cu_{68}Al_{16}Zn_{16}$ and $Cu_{73}Al_{15}Mn_{12}$, were investigated under compression tests at room temperature. The latent heat measured by DSC was $4.3\,J\,g^{-1}$ for CuAlZn and $5.0\,J\,g^{-1}$ for CuAlMn. The maximum adiabatic change of temperature during unloading was observed to be 4.0 K under 3.5% strain for CuAlZn, and 3.9 K under 4.0% strain for CuAlMn. For a cooling system application with 10 K system temperature lift, the COP_{mat} of CuAlMn is 13.3, corresponding to 0.46 of Carnot cycle COP. In general, CuAlMn is more promising than CuAlZn. CuAlMn has a 70% less transformation stress, which is more applicable in future elastocaloric cooling systems. The ultra-low hysteresis of CuAlMn not only distinguishes its COP_{mat} from CuAlZn, but also approaches the COP_{mat} of NiTi. Nevertheless, its low ΔT_{ad} is still a limitation for real-world application. In addition, cracks found after compression for CuAlZn suggested that it may not be a good SMA to be used under compression mode. Unfortunately, there are still significant gaps between the latent heat and ΔT_{ad}, indicating significant room for improvement in the future. In addition, when compared with the prior-art NiTi alloy, the latent heat of the studied two Cu-based SMAs is less than 50% of the latent heat of NiTi. Finding or synthesizing more SMAs for a larger latent heat is still needed to be competitive with NiTi and to be applicable in a real cooling system.

Authors' contributions. S.Q. and Y.G. contributed equally to the design of the DSC experiment, compression testing, elastocaloric effect testing, model validation and preparation of the manuscript. Y.W. participated in the DSC experiment, compression testing and elastocaloric effect testing. T.E.P. participated in the design of compression test set-up. Y.Ha., Y.Ya. and K.F. participated in the synthesis of CuAlMn alloys. Y.Yu. and K.T. prepared the single-crystal CuAlMn sample for this work. Y.Hw. and R.R. participated in the model validation part. J.C. contributed to the design of the whole experiment. I.T. is the PI for this project. All authors gave final approval for publication.

Competing interests. The authors declare that they have no competing interests.

Funding. The authors gratefully acknowledge the support from U.S. DOE (ARPA-E DEAR0000131) and the Center for Environmental Energy Engineering (CEEE) at the University of Maryland.

Acknowledgements. The authors acknowledge Drew Stasak for running the WDS measurements for this work. We acknowledge Shinko Metal Products Co. Ltd, International Copper Association and Japan Copper Development Association for the CuMnAl single-crystal sample.

References

1. Gschneidner Jr KA, Pecharsky V, Tsokol A. 2005 Recent developments in magnetocaloric materials. *Rep. Prog. Phys.* **68**, 1479. (doi:10.1088/0034-4885/68/6/R04)
2. Planes A, Mañosa L, Acet M. 2009 Magnetocaloric effect and its relation to shape-memory properties in ferromagnetic Heusler alloys. *J. Phys. Condensed Matter* **21**, 233201. (doi:10.1088/0953-8984/21/23/233201)

3. Smith A, Bahl CR, Bjørk R, Engelbrecht K, Nielsen KK, Pryds N. 2012 Materials challenges for high performance magnetocaloric refrigeration devices. *Adv. Energy Mater.* **2**, 1288–1318. (doi:10.1002/aenm.201200167)
4. Mischenko A, Zhang Q, Scott J, Whatmore R, Mathur N. 2006 Giant electrocaloric effect in thin-film $PbZr_{0.95}Ti_{0.05}O_3$. *Science* **311**, 1270–1271. (doi:10.1126/science.1123811)
5. Moya X, Stern-Taulats E, Crossley S, González-Alonso D, Kar-Narayan S, Planes A, Mañosa L, Mathur ND. 2013 Giant electrocaloric strength in single-crystal $BaTiO_3$. *Adv. Mater.* **25**, 1360–1365. (doi:10.1002/adma.201203823)
6. Mañosa L, González-Alonso D, Planes A, Bonnot E, Barrio M, Tamarit J-L, Aksoy S, Acet M. 2010 Giant solid-state barocaloric effect in the Ni-Mn-In magnetic shape-memory alloy. *Nat. Mater.* **9**, 478–481. (doi:10.1038/nmat2731)
7. Manosa L, Gonzalez-Alonso D, Planes A, Barrio M, Tamarit J-L, Titov IS, Acet M, Bhattacharyya A, Majumdar S. 2011 Inverse barocaloric effect in the giant magnetocaloric La–Fe–Si–Co compound. *Nat. Commun.* **2**, 595. (doi:10.1038/ncomms1606)
8. Yuce S *et al.* 2012 Barocaloric effect in the magnetocaloric prototype $Gd_5Si_2Ge_2$. *Appl. Phys. Lett.* **101**, 071906. (doi:10.1063/1.4745920)
9. Bonnot E, Romero R, Mañosa L, Vives E, Planes A. 2008 Elastocaloric effect associated with the martensitic transition in shape-memory alloys. *Phys. Rev. Lett.* **100**, 125901. (doi:10.1103/PhysRevLett.100.125901)
10. Bechtold C, Chluba C, De Miranda RL, Quandt E. 2012 High cyclic stability of the elastocaloric effect in sputtered TiNiCu shape memory films. *Appl. Phys. Lett.* **101**, 091903. (doi:10.1063/1.4748307)
11. Xiao F, Fukuda T, Kakeshita T. 2013 Significant elastocaloric effect in a Fe–31.2 Pd (at.%) single crystal. *Appl. Phys. Lett.* **102**, 1914. (doi:10.1063/1.4803168)
12. Cui J. 2014 Shape memory alloys and their applications in power generation and refrigeration. In *Mesoscopic phenomena in multifunctional materials* (eds A Saxena, A Planes), pp. 289–307. Berlin, Germany: Springer.
13. Cui J, Wu Y, Muehlbauer J, Hwang Y, Radermacher R, Fackler S, Wuttig M, Takeuchi I. 2012 Demonstration of high efficiency elastocaloric cooling with large δT using NiTi wires. *Appl. Phys. Lett.* **101**, 073904. (doi:10.1063/1.4746257)
14. Mañosa L, Jarque-Farnos S, Vives E, Planes A. 2013 Large temperature span and giant refrigerant capacity in elastocaloric Cu-Zn-Al shape memory alloys. *Appl. Phys. Lett.* **103**, 211904. (doi:10.1063/1.4832339)
15. Pataky GJ, Ertekin E, Sehitoglu H. 2015 Elastocaloric cooling potential of NiTi, Ni_2FeGa, and CoNiAl. *Acta Mater.* **96**, 420–427. (doi:10.1016/j.actamat.2015.06.011)
16. Nikitin S, Myalikgulyev G, Annaorazov M, Tyurin A, Myndyev R, Akopyan S. 1992 Giant elastocaloric effect in FeRh alloy. *Phys. Lett. A* **171**, 234–236. (doi:10.1016/0375-9601(92)90432-L)
17. Rodriguez C, Brown LC. 1980 The thermal effect due to stress-induced martensite formation in β-CuAlNi single crystals. *Metall. Mater. Trans. A* **11**, 147–150. See http://link.springer.com/article/10.1007/BF02700450.
18. Brown L. 1981 The thermal effect in pseudoelastic single crystals of β-CuZnSn. *Metall. Trans. A* **12**, 1491–1494. (doi:10.1007/BF02643695)
19. Xiao F, Jin M, Liu J, Jin X. 2015 Elastocaloric effect in $Ni_{50}Fe_{19}Ga_{27}Co_4$ single crystals. *Acta Mater.* **96**, 292–300. (doi:10.1016/j.actamat.2015.05.054)
20. Annaorazov M, Nikitin S, Tyurin A, Asatryan K, Dovletov AK. 1996 Anomalously high entropy change in FeRh alloy. *J. Appl. Phys.* **79**, 1689–1695. (doi:10.1063/1.360955)
21. Zak G, Kneissl AC, Zatulskij G. 1996 Shape memory effect in cryogenic Cu-Al-Mn alloys. *Scr. Mater.* **34**, 363–367. (doi:10.1016/S0956-716X(95)00531-Y)
22. Mielczarek A, Riehemann W, Vogelgesang S, Tonn B. 2008 Mechanical and fatigue properties of Cu-Al-Mn shape memory alloys with influence of mechanical cycling on amplitude dependence of internal friction at room temperature. In *Interaction between defects and anelastic phenomena in solids* (eds IS Golovin, DM Levin). Solid State Phenomena, vol. 137, pp. 145–154. Pfaffikon, Switzerland: Trans Tech Publications. (doi:10.4028/www.scientific.net/SSP.137.145)
23. Zak G, Prader P, Kneissl A. 1995 Gefüge und Eigenschaften von Cu-Al-Mn-Formgedächtnislegierungen. *Metall* **49**, 415–418.

24. Kainuma R, Takahashi S, Ishida K. 1996 Thermoelastic martensite and shape memory effect in ductile Cu-Al-Mn alloys. *Metall. Mater. Trans. A* **27**, 2187–2195. (doi:10.1007/BF02651873)
25. Qian S, Wu Y, Ling J, Muehlbauer J, Hwang Y, Takeuchi I, Rademacher R. 2015 Design, development and testing of a compressive thermoelastic cooling system. Presented at *The 24th IIR Int. Congr. of Refrigeration* (*ICR2015*), *Improving Quality of Life, Preserving the Earth, Yokohama, Japan, 16–22 August 2015*. Paper B1-We-1b 92.
26. Huang W. 2002 On the selection of shape memory alloys for actuators. *Mater. Des.* **23**, 11–19. (doi:10.1016/S0261-3069(01)00039-5)
27. Ziolkowski A. 2015 *Pseudoelasticity of shape memory alloys: theory and experimental studies*. London, UK: Butterworth-Heinemann.
28. Qian S, Ling J, Muehlbauer J, Hwang Y, Radermacher R. 2015 Study on high efficient heat recovery cycle for solid-state cooling. *Int. J. Refrig.* **55**, 102–119. (doi:10.1016/j.ijrefrig.2015.03.023)
29. Qian S, Ling J, Hwang Y, Radermacher R, Takeuchi I. 2015 Thermodynamics cycle analysis and numerical modeling of thermoelastic cooling systems. *Int. J. Refrig.* **56**, 65–80. (doi:10.1016/j.ijrefrig.2015.04.001)
30. Qian S, Nasuta D, Rhoads A, Wang Y, Geng Y, Hwang Y, Radermacher R, Takeuchi I. 2016 Not-in-kind cooling technologies: a quantitative comparison of refrigerants and system performance. *Int. J. Refrig.* **62**, 177–192. (doi:10.1016/j.ijrefrig.2015.10.019)